Polymer Testing 126 (2023) 108158

Contents lists available at ScienceDirect

Polymer Testing

journal homepage: www.elsevier.com/locate/polytest

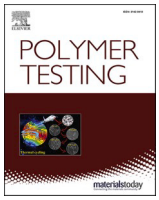

Effects of nano-sized $BaTiO_3$ on microstructural, thermal, mechanical and piezoelectric behavior of electrospun PVDF/$BaTiO_3$ nanocomposite mats

Mateja Kubin [a], Petre Makreski [b], Michele Zanoni [c], Leonardo Gasperini [d], Giacomo Selleri [d], Davide Fabiani [d,e], Chiara Gualandi [c,e], Aleksandra Bužarovska [a,*]

[a] Ss. Cyril and Methodius University, Faculty of Technology and Metallurgy, Rudjer Boskovic 16, 1000, Skopje, Macedonia
[b] Ss. Cyril and Methodius University in Skopje, Faculty of Natural Sciences and Mathematics, Institute of Chemistry, Arhimedova 5, 1000, Skopje, Macedonia
[c] Department of Chemistry "Giacomo Ciamician" and INSTM UdR of Bologna, University of Bologna, Via Selmi, 2, 40126, Bologna, Italy
[d] Department of Electrical, Electronic, and Information Engineering, University of Bologna, Viale Risorgimento 2, 40136, Bologna, Italy
[e] Interdepartmental Center for Industrial Research on Advanced Applications in Mechanical Engineering and Materials Technology, CIRI-MAM, University of Bologna, Viale Risorgimento, 2, 40136, Bologna, Italy

ARTICLE INFO

Keywords:
PVDF
β-phase
Crystallinity
Barium titanate
Piezoelectric properties

ABSTRACT

Polyvinylidene fluoride (PVDF) is a good candidate for use in wearable electronics due to its flexibility, ease of processing, and ability to generate electrical charge in response to applied mechanical stress. In this work, low-density polyvinylidene fluoride (PVDF) nanocomposites containing nano-sized $BaTiO_3$ with cubic symmetry were fabricated by electrospinning process, aiming to generate dominant electroactive β polar phase. The influence of nano-sized filler content on the microstructure, total degree of crystallinity, β phase content, and piezoelectric properties of the electrospun PVDF/$BaTiO_3$ nanocomposites was systematically studied. The crystallinity and the thermal stability were evaluated using differential scanning calorimetry (DSC), x-ray diffraction (XRD) and thermogravimetric analysis (TGA). The content of evolved piezoactive β phase was determined by FTIR spectroscopy. It was shown that the electrospinning process is primarily responsible for very high content (up to 99.4%) of the developed piezoactive crystalline phase. High degree of crystallinity (up to 56.4%) was determined in PVDF/$BaTiO_3$ nanocomposites, confirming the nucleation ability of the nanofiller. Maximum tensile strength of 55.5 MPa (127% higher than PVDF nanofiber mat) and maximum d_{33} coefficient of 18 pC N^{-1} were determined for the nanofiber mat containing 20 wt% $BaTiO_3$. We believe that this work provides an important insight into the nanoparticles' distribution and their agglomeration (SEM and TEM analyses) influence on the final properties of PVDF/$BaTiO_3$ webs, generated via electrospinning.

1. Introduction

Piezoelectric materials have attracted much attention in research on small-scale electronic devices, including portable energy collectors, self-powered devices, and devices for environmental and human health monitoring, due to their distinct ability to convert mechanical energy into electrical energy [1]. As a typical piezoelectric material with intrinsic flexibility, poly(vinylidene fluoride) (PVDF) has been extensively studied as a core material for the aforementioned devices [2]. PVDF can crystallize in five different polymorphs, known as α, β, γ, δ, and ε, of which the β phase exhibits the highest piezoelectric activity [3,4]. In general, PVDF mainly crystallizes in the α phase, which is unfavorable due to its non-polar character and lack of piezoelectric activity. The development of a high β phase content is primarily dependent on the processing conditions and post-processing methods such as mechanical stretching and electrical poling treatments [5]. Recently, electrospinning has emerged as a promising processing route for achieving high β phase content in this ferroelectric polymer. Electrospinning offers the advantage of simultaneous mechanical stretching and electrical poling of the fibers since this technique uses high electric fields [6]. Electrospun nanofibers possess unique properties such as high surface area per unit mass, combined with high porosity and excellent flexibility [7]. Furthermore, due to the high β phase content, electrospun PVDF fibers display a larger piezoelectric response in comparison with PVDF thin films fabricated using solvent casting techniques [8].

However, piezoelectric polymers display low piezoelectric

* Corresponding author.
E-mail address: abuzar@tmf.ukim.edu.mk (A. Bužarovska).

https://doi.org/10.1016/j.polymertesting.2023.108158
Received 22 May 2023; Received in revised form 4 July 2023; Accepted 25 July 2023
Available online 27 July 2023

coefficients compared to piezo ceramics. Various additives have been used to further enhance the piezoelectric activity of polymer fibers. Accordingly, prepared electrospun PVDF fibers were modified with various fillers such as carbon nanotubes, graphene sheets, and ceramic nanoparticles [9–11]. Among ceramic piezoelectric materials, $BaTiO_3$ was found to be a promising additive because it has a high piezoelectric strain coefficient, which enables greater energy transfer when used in energy harvesting devices and sensors [12]. It is also an environmentally friendly material and can be incorporated into biomedical devices.

The addition of $BaTiO_3$ to PVDF fibers has been shown to modify the nanofibers' morphology, increase the β phase content, and improve the piezoelectric and sensing capabilities of the fibers, while maintaining the desired flexibility [13,14]. Guo et al. fabricated a piezoelectric pressure sensor based on PVDF/$BaTiO_3$ nanocomposite fibers with excellent output voltage values resulting from the addition of $BaTiO_3$ nanowires [15]. In another study, electrospun nanocomposite fiber mats of PVDF combined with graphene nanosheets and $BaTiO_3$ nanoparticles were employed as a piezoelectric nanogenerator, achieving an output voltage of 11 V and electric power of 4.1 μW [16]. A piezoelectric nanogenerator was also prepared by introducing a hybrid structure of ZnO nanorods and $BaTiO_3$ nanospheres into PVDF fibers, resulting in improved crystallization and high piezoelectric output voltage [17]. Most of the reference research in this field was mainly devoted to phase analysis and quantification of individual crystal phases, while giving limited focus on the overall degree of crystallinity. This is of high importance, since the "content of effective piezo-phase" (C_{ep}) is a product of the overall degree of crystallinity, and the β phase content, directly influencing the piezoelectric response of the composites. Processing routes and conditions, as well as the distribution of the nano-sized fillers, are other important aspects, relevant for controlling the phase fractions of the crystalline form.

Therefore, this work provides a comprehensive study on the effect of nano-sized $BaTiO_3$ (in cubic crystal phase) on the microstructure, thermal, mechanical and piezoelectric behavior of the electrospun PVDF/$BaTiO_3$ nanocomposite mats. Particular attention was given to the distribution of nano-sized filler (SEM and TEM analyses) within electrospun PVDF fibers, and its influence on the final nanocomposite properties.

2. Materials and methods

2.1. Materials

Poly(vinylidene difluoride) (PVDF) (Solef 6008) with a melt mass-flow rate of 5.5–11 g/10 min (measured at 230 °C with 2.16 kg according to ASTMD1238), was supplied by Solvay Specialty Polymers (Italy). Barium titanate ($BaTiO_3$) nanopowder with a particle size <100 nm and 99% purity was purchased from Sigma-Aldrich. Dimethyl sulfoxide (DMSO) and acetone (Ac) (Merck products) were used as solvents without previous purification.

2.2. Preparation of PVDF/$BaTiO_3$ nanofibers

Polymer nanofiber mats were prepared by electrospinning technique, using a solvent mixture of DMSO and acetone (60/40 v/v). First, $BaTiO_3$ nanoparticles were dispersed in DMSO in the appropriate amount (5, 10, 15, and 20 wt% with respect to the polymer) and sonicated for 90 min. PVDF powder and acetone were then added to the dispersion to obtain the desired polymer concentration, i.e. 20 wt% in dispersions with 5 and 10 wt% $BaTiO_3$ and 18 wt% in dispersions with 15 and 20 wt% of $BaTiO_3$. It is important to note that PVDF concentration within the dispersions with higher nanoceramics content was lowered for 10% in order to achieve a stable electrospinning process. Dissolution of PVDF (in the corresponding dispersion was performed by mechanically stirring overnight at 70 °C. Finally, the polymer dispersions were additionally sonicated for 1 h before electrospinning to improve the dispersion of nanoparticles. A pure PVDF nanofiber mat was electrospun as a reference. A horizontal electrospinning setup (Spinbox, Bioinicia S.L.) with a flat collector (20 × 20 cm) was used to produce nanocomposite mats. A schematic representation of the process is shown in Fig. 1. The prepared polymer dispersion was loaded in a 5 mL plastic syringe with a 20 GA needle. Electrospinning was performed at a flow rate of 0.8 mL h^{-1}, maintaining a constant distance of 23 cm between the emitter and the collector, and applying a spinning voltage of 16 kV for the pure polymer and 19 kV for the PVDF/$BaTiO_3$ composites. The electrospun mats were vacuum-dried overnight at 40 °C. The PVDF/$BaTiO_3$ nanocomposite mats are denoted as ES-PVDF-X, where X (5, 10, 15, 20) represents the weight percentage of $BaTiO_3$.

2.3. Poling process of electrospun samples

In a traditional contact poling technique, the high porosity of the nanofibrous membranes could trigger electrical breakdown through the air gaps between the nanofibers, as an external electric field is applied. Therefore, an embedding medium was required during the process, as described in detail in Ref. [18]. The prepared nanocomposite mats were polarized in an oil bath (FR3 natural ester, Cargill) at 120 °C with an electric field of 20 kV mm^{-1} for 1 h. Before poling, the samples (2 × 2 cm) were placed in a vacuum chamber to impregnate the oil inside the fibers. After poling, the nanofiber mats were immersed in cyclohexane for 1 h to remove the remaining oil. To remove residual electrostatic charges which could affect the measurement of the piezoelectric properties, the two opposite surfaces of the specimens were connected to the ground for 24 h.

2.4. Characterization of electrospun mats

The morphology of the electrospun samples was observed using a scanning electron microscope (SEM, Leica Cambridge Stereoscan 360) with an accelerating voltage of 20 kV. Prior to characterization, the nanofiber mats were coated with gold. The distribution of fiber diameters was determined through the measurement of about 150 fibers and the results are given as the average diameter ± standard deviation. The Student's t-test was used to verify the statistical significance of the difference between the mean values ($p < 0.001$).

Transmission Electron Microscopy (TEM) observations were carried out by using a Philips microscope with an acceleration voltage of 80 kV.

The density and porosity of the prepared mats were determined by the liquid displacement method using ethanol as a medium [19]. The density and porosity were calculated using the following equations, respectively:

$$\rho = \frac{W}{V_2 - V_3} \quad (1)$$

$$\varepsilon = \frac{V_1 - V_3}{V_2 - V_3} \times 100 \quad (2)$$

where W is the weight of the electrospun mat, V_1 is the known volume of ethanol in the glass vial, V_2 is the total volume of ethanol where ethanol-impregnated mat is immersed, and V_3 is the volume of residual ethanol after removal of the ethanol-impregnated electrospun mat.

The ATR-FTIR spectra were recorded in a range of 4000-400 cm^{-1}, with 32 scans and a resolution of 4 cm^{-1} using an IRAffinity-1S spectrometer (Shimadzu, Japan).

The crystalline structure of the nanofibers was analyzed using XRD (Rigaku Ultima IV powder X-ray diffractometer) with CuK_α radiation ($\lambda = 0.154$ nm) operated at 40 kV and 40 mA. Diffractograms were recorded at room temperature in the 2θ range between 10 and 80° and a scanning rate of 0.02 °min^{-1}.

The thermal behavior of the electrospun fibers was monitored by differential scanning calorimetry (DSC) using PerkinElmer Differential Scanning Calorimeter DSC 7, under nitrogen atmosphere. Samples of

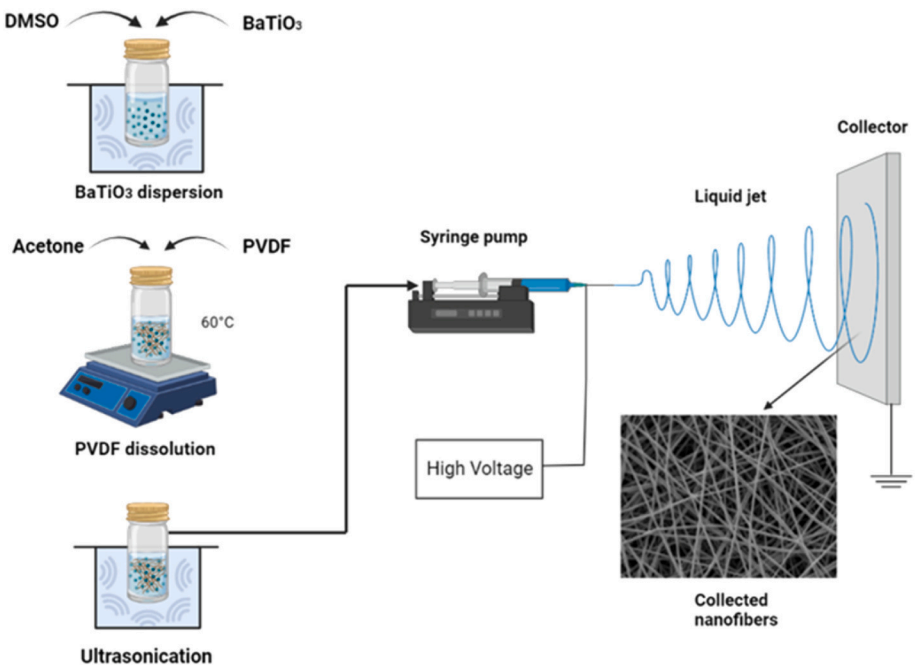

Fig. 1. Scheme of preparation of electrospun PVDF/$BaTiO_3$ nanofiber mats.

approximately 8 mg weight were first heated from 20 °C to 200 °C at a heating rate of 10 °C min^{-1} and kept at final temperature for 1 min. Subsequently, the samples were cooled to 20 °C at a cooling rate of 10 °C min^{-1} and reheated to 200 °C at the same heating rate of 10 °C min^{-1}. The degree of crystallinity was calculated using the following equation:

$$X_c = \left(\frac{\Delta H_m}{\Delta H_m^o \times \left(1 - \frac{wt.\%\ BaTiO_3}{100}\right)} \right) \times 100 \quad (3)$$

where ΔH_m is melting enthalpy, ΔH_m^o is the enthalpy of hypothetically 100% crystallized PVDF, which is reported to be 104.7 J g^{-1} [20], and wt.% $BaTiO_3$ is the weight percentage of ceramic nanoparticles.

Thermogravimetric analysis was performed using TGA Q500 (TA instruments) under constant air flow. Measurements were performed from room temperature to 600 °C with a heating rate of 10 °C min^{-1}.

The mechanical properties of the PVDF/$BaTiO_3$ nanocomposite mats were investigated by tensile testing using a Shimadzu AGS-X tester at a test rate of 10 mm min^{-1}. Five samples of each nanofiber mat (2 × 7 cm) were weighed and tested. Young's modulus, maximum value of stress (σ_{max}) and strain at maximum stress ($\varepsilon_{\sigma\ max}$) were determined as an average value of the tested samples.

The piezoelectric properties of the electrospun mats were evaluated by measuring the piezoelectric strain coefficient d_{33} (pC N^{-1}). The d_{33} coefficient was measured with a piezometer (d_{33} PiezoMeter System PM300, Piezotest, Singapore) by compressing the samples with an oscillating sinusoidal force between 0.25 and 0.5 N at 110 Hz.

3. Results and discussion

3.1. Morphology of electrospun PVDF/$BaTiO_3$ composite mats

SEM images of the electrospun nanofiber mats are presented in Fig. 2. The unfilled PVDF nanofibers with an average diameter of 500 ± 170 nm showed a smooth and bead-free morphology (Fig. 2a and b). On the other hand, the PVDF nanofibers filled with ceramic nanoparticles at a concentration higher than 5 wt% showed rough surfaces and an increasing amount of bulges as the content of $BaTiO_3$ rises. These irregularities may be agglomerates of ceramic nanoparticles protruding out of the fibers as the concentration of the filler increases. This was confirmed by TEM observation (Fig. 3) showing that ES-PVDF-5 mostly contains single $BatiO_3$ nanoparticles distributed across the bulk and the surface of the fibers, while the amount of aggregated particles rises steadily in the other samples.The inclusion of $BaTiO_3$ in the initial polymser solution produces a dramatic decrease in fiber diameters, with the fibers being almost halved when the concentration is 10 and 15.wt% (ES-PVDF-5 vs ES-PVDF-10 not significant, $p > 0.05$), it further reduces in ES-PVDF-15, while it rises in ES-PVDF-20, although it is lower than the unfilled sample. The drop of fiber diameter in the nanocomposites is probably ascribable to the high dielectric constant of $BaTiO_3$, as previously found [21].

3.2. Density and porosity of PVDF/$BaTiO_3$ nanofiber mats

The porosity and density data for the electrospun samples are summarized in Table 1. It can be seen that all the electrospun samples have a high degree of porosity (above 90%) and a relatively low density (about 0.08 g cm^{-3}). The addition of ceramic nanoparticles did not affect the density of the nanofiber mats. On the other hand, a slight decrease in porosity was observed with the addition of $BaTiO_3$ nanoparticles. Similar observations were identified in nanocomposite fibers with MWCNTs and clay particles [9,22].

3.3. FTIR-ATR analysis and β phase content

FTIR spectroscopy has proven to be a useful tool for the assessment of different crystal polymorphs developed in PVDF [3]. The FTIR spectra of electrospun PVDF and its nanocomposites with $BaTiO_3$ are presented in Fig. 4. The bands at 509 cm^{-1} (CF_2 bending), 839 cm^{-1} (CH_2 rocking), and 1431 cm^{-1} (CH_2 bending), which are clearly seen in all spectra, are usually associated with the β phase [3,23]. The presence of α phase is usually related with the band at 764 cm^{-1}, belonging to CF_2 bending vibration [3,23]. In all presented spectra, this band has a very low intensity, while additional peaks characteristic of the α phase barely emerge. Some confusion may arise when assigning the vibrational bands of β- and γ-forms in PVDF, since these crystal polymorphs display very close spectral features. The band at 839 cm^{-1}, arising from CH_2 rocking, can be assigned to both β and γ polymorphs, since this vibration

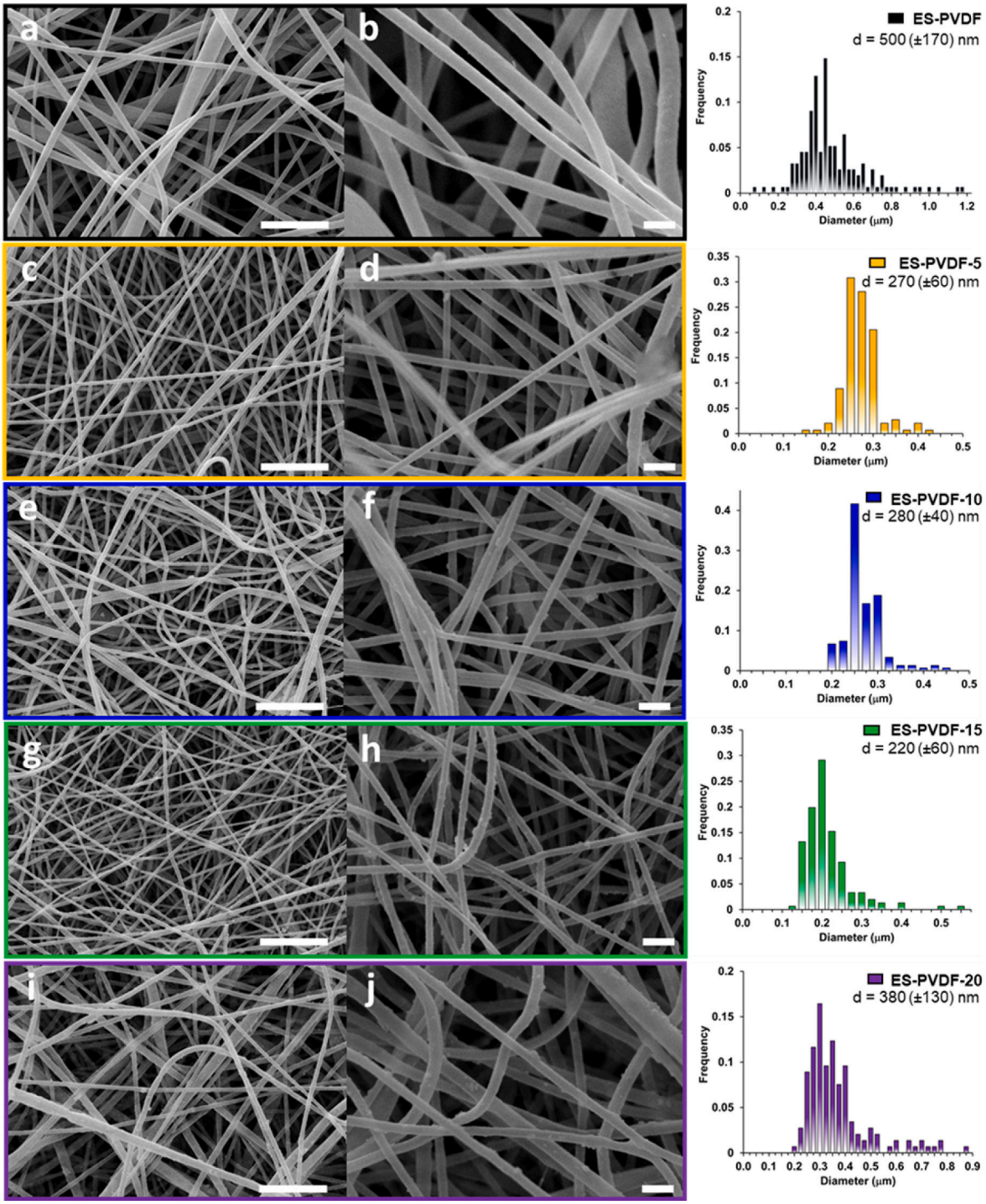

Fig. 2. SEM images of electrospun PVDF/$BaTiO_3$ nanocomposite fibers: ES-PVDF (a, b), ES-PVDF-5 (c, d), ES-PVDF-10 (e, f), ES-PVDF-15 (g, h), ES-PVDF-20 (i, j), and corresponding fiber diameter distributions. Scale bars: 5 μm (a, c, e, g, i) and 1 μm (b, d, f, h, j).

originates from macromolecular chains with a longer trans sequence than TT, which is common for the all-trans (TTTT) conformation of the β phase and the TTTGTTTG' conformation of the γ phase [24]. According to the literature, these phases can be distinguished by exclusive peaks at 1275 cm^{-1} for β phase and 1236 cm^{-1} for the γ phase [23]. A distinct band at 1275 cm^{-1} was observed in all spectra, confirming the dominant presence of the β phase, while a minor absorbance can be seen at 1236 cm^{-1} arising from the γ phase.

Accordingly, the relative content of the β and γ phases can be calculated by examining the absorbance band position at 839 cm^{-1} and absorbance bands present at 1275 cm^{-1} and 1236 cm^{-1} using the following equations:

$$F_{EA} = \frac{A_{EA}}{\left(\frac{K_{839}}{K_{764}}\right)A_{764} + A_{EA}} = \frac{A_{EA}}{1.26A_{764} + A_{EA}} \times 100 \quad (4)$$

where F_{EA} represents the content of electroactive phase, the absorption coefficients, K_{764} and K_{839} are 6.1x10^4 and 7.7 × 10^4 cm^2 mol^{-1}, while A_{764} and A_{EA} are absorbance values at 764 cm^{-1} and 839 cm^{-1}, respectively [24], and

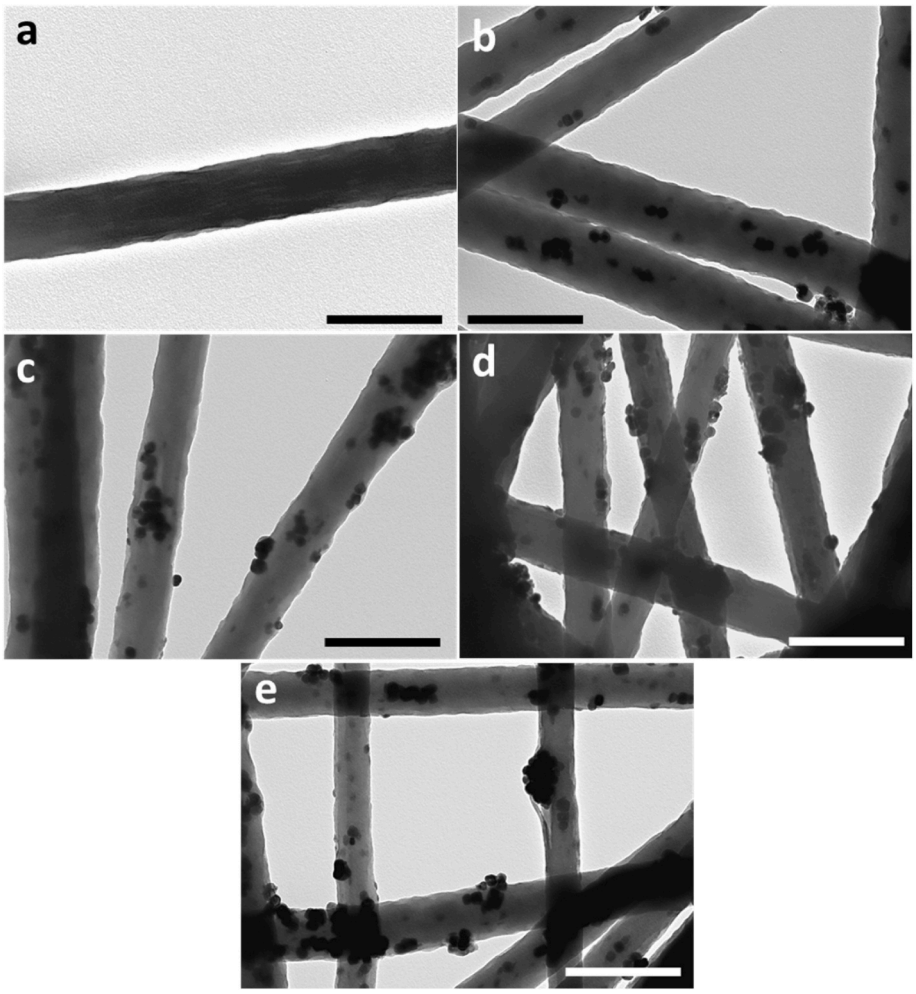

Fig. 3. TEM images of electrospun PVDF/$BaTiO_3$ nanocomposite fibers: ES-PVDF (a), ES-PVDF-5 (b), ES-PVDF-10 (c), ES-PVDF-15 (d), and ES-PVDF-20 (e). Scale bar: 500 nm.

Table 1
Density and porosity data of PVDF/$BaTiO_3$ nanofiber mats.

Sample	ρ[a] [g cm^{-3}]	ε[b] [%]
ES-PVDF	0.08 ± 0.02	96.0 ± 0.02
ES-PVDF-5	0.11 ± 0.04	92.5 ± 0.02
ES-PVDF-10	0.08 ± 0.02	94.2 ± 0.05
ES-PVDF-15	0.07 ± 0.01	94.7 ± 0.01
ES-PVDF-20	0.09 ± 0.01	90.3 ± 0.01

[a] Calculated by applying Equation 1.
[b] Calculated by applying Equation 2.

$$F(\beta) = F_{EA} \times \left(\frac{\Delta H_\beta}{\Delta H_\beta + \Delta H_\gamma}\right) \times 100 \quad (5)$$

$$F(\gamma) = F_{EA} \times \left(\frac{\Delta H_\gamma}{\Delta H_\beta + \Delta H_\gamma}\right) \times 100 \quad (6)$$

where, ΔH_β and ΔH_γ are the height differences between the peak positioned at 1275 cm^{-1} and the nearest valley close to 1260 cm^{-1}, and the peak positioned at 1236 cm^{-1} and the nearest valley around 1225 cm^{-1} [23].

Calculations performed using Equation (4) gives the information of the relative amount of the both electroactive phases (β or γ) compared to the nonpolar α phase, while further analysis of the exclusive peaks of these phases positioned in the region 1220-1290 cm^{-1} (inset of Fig. 4) enables to separate the two electroactive phases (Equations (5) and (6)).

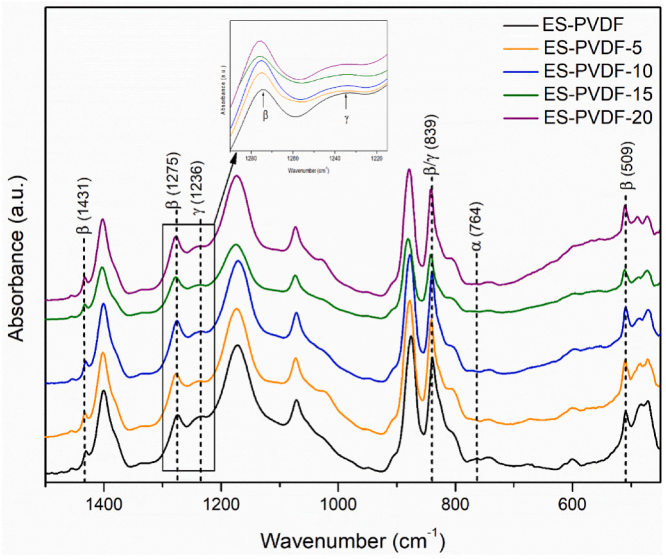

Fig. 4. FTIR spectra of electrospun PVDF/$BaTiO_3$ nanocomposite fibers. Inset: FTIR region of 1290-1220 cm^{-1}.

Table 2
Content of electroactive phases and degree of crystallinity determined by FTIR and XRD analyses.

Sample	F_{EA}[a] [%]	F(β)[b] [%]	F(γ)[c] [%]	X_c[d] [%]
ES-PVDF	97.0	88.7	8.3	36.5
ES-PVDF-5	98.4	91.0	7.4	56.4
ES-PVDF-10	97.9	92.1	5.8	52.0
ES-PVDF-15	98.4	91.0	7.4	41.9
ES-PVDF-20	99.4	95.5	3.9	53.7

[a] Calculated by applying Equation 4.
[b] Calculated by applying Equation 5.
[c] Calculated by applying Equation 6.
[d] Calculated by applying Equation 7.

The calculated relative contents of the electroactive phases and individual contents of β and γ phases are presented in Table 2. A remarkable content of electroactive phases, (up to 99.4%) is achieved in all electrospun samples. The individual phase calculations showed that this high content is mainly due to β phase. The content of γ phase ranges from 3.9 to 8.3%, appearing lowest for the sample with 20 wt% $BaTiO_3$ nanoparticles. A high percentage of β phase is present in the pure electrospun PVDF sample as well as in the composites, indicating that the electrospinning process has a greater influence on the developed β phase than the nanoparticle content. In particular, the stretching of the electrospinning jet accompanied by the local poling effect induced by the applied high voltage contributed to the alignment of the polymer chains in the all-trans conformation characteristic of the β phase [9]. The choice of a polar solvent, such as DMSO may also affect the enhancement of the β phase content due to its dipolar interactions with the polymer chains [25]. The addition of $BaTiO_3$ nanoparticles led to a minor increase in the presence of β phase, likely due to their ability to restrict the polymer chains from relaxing and enhance the crystallization of the β phase [14,26]. Hence, the high β phase in the nanocomposite fibers seems to be the result of a synergistic effect between the applied voltage during electrospinning and the addition of nanoparticles.

effect between the applied voltage during electrospinning and the addition of nanoparticles.

3.4. X-ray diffraction analysis

X-ray diffraction analysis was performed to investigate the structural features of the electrospun samples and to calculate the degree of crystallinity. The XRD patterns are shown in Fig. 5a. A distinct peak at 20.6° corresponding to the (200/110) reflection of the orthorhombic β phase can be seen in all samples [16,23,27]. An additional well-defined peak at 36.3° was also detected, corresponding to the β phase in PVDF [16,23,27]. Diffraction peaks relevant to the perovskite structure of $BaTiO_3$ and belonging to the orientation planes (100), (110), (111), and (200) were clearly observed at 22.2°, 31.5°, 38.9°, and 45.3°, respectively. Their intensities increased with the increase of the content of $BaTiO_3$ in the corresponding composites [28].

The XRD analysis data confirmed that the prepared samples were mainly crystallized in the β phase, as no diffraction peaks belonging to the α and γ phases could be detected. Correlating with the FTIR results, the low amount of α and γ phases calculated by the FTIR analysis is probably insufficient to be seen in the diffractograms. Furthermore, the degree of crystallinity of the samples was determined using the following equation:

$$X_c = \frac{\sum A_c}{\sum A_c + \sum A_a} \times 100 \quad (7)$$

Where, ΣA_c and ΣA_a represent the total integrated areas of the polymer crystalline peaks and the amorphous halo, respectively. Curve-fitting was performed using Grams AI™ Spectroscopy software to properly integrate the peaks and amorphous halo (Fig. 5b). Accordingly, the calculated degrees of crystallinity are shown in Table 2. The lowest crystallinity of 36.5% was determined for the pure PVDF sample, while the addition of $BaTiO_3$ increased the overall crystallinity of the electrospun mats. Specifically, $BaTiO_3$ nanoparticles could promote polymer crystallization, but their possible agglomeration can hinder this process and lower the overall crystallinity [29,30].

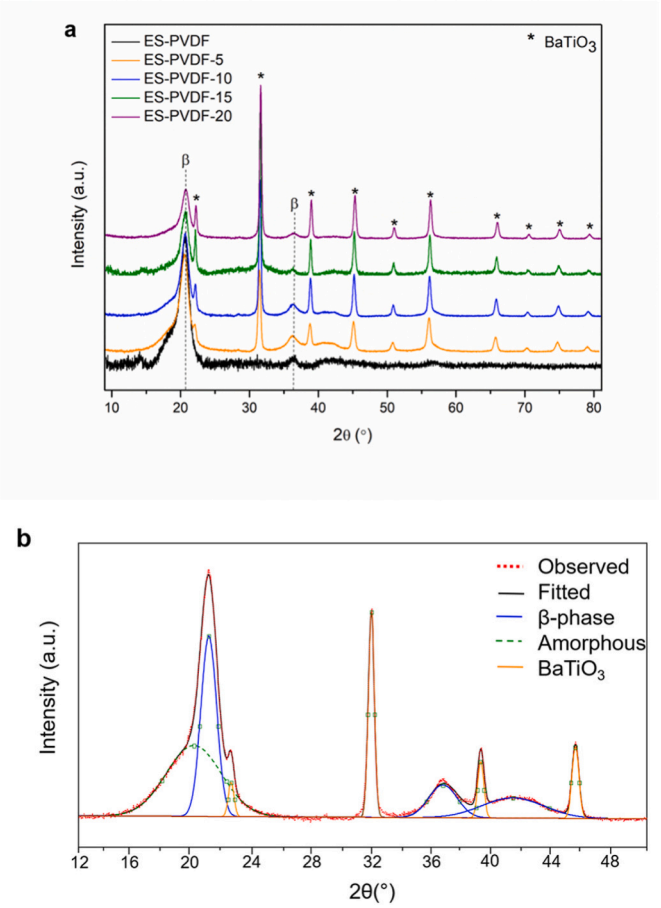

Fig. 5. XRD patterns of PVDF/$BaTiO_3$ electrospun samples (a) and curve fitting of XRD peaks in ES-PVDF-5 sample (b).

3.5. Thermal properties

TG analysis was performed to investigate the effect of $BaTiO_3$ NPs on the thermal stability of the samples and to evaluate the weight residues. The obtained TGA curves and all collected data are presented in Fig. 6 and Table 3. The two-step degradation process was characteristic for all the investigated samples. The degradation of PVDF nanofibers proceeds at 600 °C without residual weight. The residual weights of the nanocomposite mats increase with the addition of the nanoparticles, which nicely complement the nominal content of the added filler. The onset decomposition temperatures of the nanocomposite mats (Table 3) are shifted to lower values indicating that the addition of $BaTiO_3$ nanofiller decreased the thermal stability of the nanofiber composites. Similar outcomes on the influence of $BaTiO_3$ nanoparticles on the thermal degradation of PVDF have been reported previously [25].

The DSC thermograms are presented in Fig. 7 and all relevant data are summarized in Table 3. During the first heating run (Fig. 7a), a bimodal melting peak (with maxima at about 170 °C and 174 °C) is evident, followed by a low-intensity endothermic peak at a temperature above 180 °C in almost all investigated samples. An additional small endothermic peak at about 63 °C, detected only in the ES-PVDF-5 mat, is

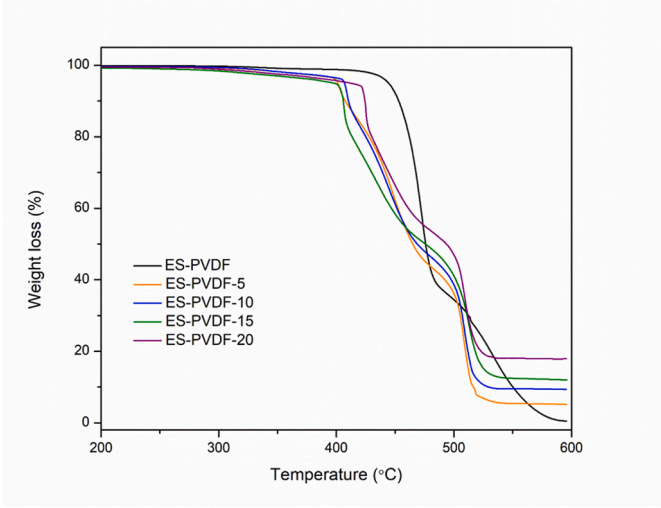

Fig. 6. Thermogravimetric analysis of electrospun samples.

usually ascribed to the organization of conformational disordered α-phase or the melting of paracrystalline domains [31,32]. The melting range of the different crystal phases of PVDF is presented in Fig. 7a. It can be seen that the bimodal peaks lay within the range of 169–174 °C that according to literature data, includes the melting temperatures of β phase (165–172 °C) and α polymorphs (172–175 °C) [3,31]. The third endothermic peak can be noticed at higher temperatures which corresponds to the melting of the γ phase. In line with the results obtained from the FTIR analysis, indeed, a small amount of α and γ phases are present, which during the first heating run, melted at different temperatures. The lowest amounts of γ phase are seen for the samples with 10 and 20 wt% $BaTiO_3$ nanoparticles, which can also be noticed in the inset of Fig. 7a, where the endotherm for these samples shows the lowest intensity.

Even though, the DSC technique offers a way to distinguish the different phases in PVDF, it is not very reliable because other factors affect the melting behavior, such as sample morphology, lamellar thickness, and crystal perfection. In some cases, double melting peaks in DSC thermograms may also arise from melting/recrystallization and remelting during heating runs [20,33].

The estimated degree of crystallinity varied between 32.1 and 51.9%. It could be noted that the degree of crystallinity increased with increasing content of $BaTiO_3$ nanoparticles but in an irregular manner. This behavior might be due to the possible changes in the quality of the PVDF-$BaTiO_3$ dispersions associated with nanoparticle agglomeration occurring during electrospinning, considering the length of the process. The obtained X_c values are in accordance with the results of XRD analysis and literature data on electrospun PVDF fibers [10,14,30,34]. Namely, the crystallites of the β-phase are smaller than those of the α-phase, thus reducing the crystallinity in β-phase rich samples [34].

The crystallization from the polymer melt was presented in Fig. 7b. A single crystallization peak at 142 °C was observed in all investigated electrospun mats showing no influence of the $BaTiO_3$ nanoparticle content. The determined crystallization enthalpies varied in the range of 48.4–58.4 J g^{-1}. During the second heating runs (Fig. 7c), the melting peaks shifted to higher temperature values (up to 175 °C), indicating melting in the α-phase, since this polymorphic form is thermodynamically more favorable during the subsequent crystallization process.

3.6. Mechanical properties

The mechanical properties of the nanofiber mats were studied by standard tensile tests. Fig. 8 shows the stress-strain curves of the tested specimens, while the values for Young's modulus, maximum value of stress (σ_{max}) and strain at maximum stress ($\varepsilon_{\sigma\ max}$) are summarized in Table 4. The tensile stress was calculated using an equation proposed by Maccaferri et al. [35]:

$$\sigma = \rho \frac{F}{m} L \tag{8}$$

where m is the mass of the sample (measured in mg), ρ is the material density, F is the force (measured in N), L is the initial length of the sample (measured in mm) and σ is the stress expressed in MPa. The density corrections of the samples were performed following the weight percentage of the nanoparticles. This type of stress calculation enables more realistic values compared to the standard approach where the cross section area of the sample is used. From the stress-strain curves (Fig. 8), it is clear that the addition of $BaTiO_3$ nanoparticles improved the mechanical properties of the mats. According to the results presented in Table 4, a negligible decrease in Young's modulus can be observed by the addition of nanoparticles. Furthermore, the ultimate tensile strength increased in all electrospun samples compared to PVDF nanofiber mat. The maximum tensile stress of 55.5 MPa was reached for the ES-PVDF-20 sample which was 127% higher than the pristine nanofiber mat. The elongation at break was found to increase with the nanoparticles content, confirming the positive effect of the nanofiller on the mechanical properties of the samples. The nanofibers presented in this study are randomly oriented since a static collector was used. During the stretching process, the nanofibers partially align in the direction of the stress. The added nanoparticles may have prevented further deformation of the nanofibers, acting as temporary cross-linkers between the polymer chains, thus producing localized regions of enhanced tensile strength and modulus [14,22].

3.7. Piezoelectric properties

The piezoelectric performance of the composite nanofibers was evaluated by measuring the piezoelectric strain coefficient d_{33} after poling. The values are listed in Table 4. The piezoelectric performance of PVDF nanofibers strongly depends on the amount of the β phase present and the total degree of crystallinity in the samples [36]. According to the values presented in Table 4, the highest piezoelectric coefficient (−18.5 pC N^{-1}) is obtained for the nanofiber mat with 20 wt% $BaTiO_3$ nanoparticles, corresponding to the highest content of β phase determined from the FTIR analysis (Table 2). However, the content of β phase

Table 3
Thermal properties of PVDF/$BaTiO_3$ nanofibers.

Sample	I run				Crystallization		II run			TGA	
	T_{m1} [°C]	T_{m2} [°C]	ΔH_m [J g^{-1}]	X^a_c [%]	T_{cr} [°C]	ΔH_{cr} [J g^{-1}]	T_{m2}[°C]	ΔH_m [J g^{-1}]	X^a_c [%]	T_{onset} [°C]	$W_{res}{}^b$ [%]
ES-PVDF	170	174	40.3	38.5	141	−38.4	174	40.8	38.9	450	0.5
ES-PVDF-5	169	173	51.8	51.9	142	−48.0	174	52.3	52.4	401	5.2
ES-PVDF-10	170	174	45.7	48.0	142	−44.9	175	47.3	49.7	403	9.4
ES-PVDF-15	169	–	29.2	32.1	142	−41.8	174	40.8	44.8	404	12.0
ES-PVDF-20	170	173	42.3	48.4	142	−40.4	174	40.0	45.9	421	17.9

[a] Calculated by applying Equation (3), where wt.%$BaTiO_3$ is 4.7, 9.1, 13 and 16.7% for ES-PVDF-5, ES-PVDF-10, ES-PVDF-15 and ES-PVDF-20, respectively.
[b] At 600 °C.

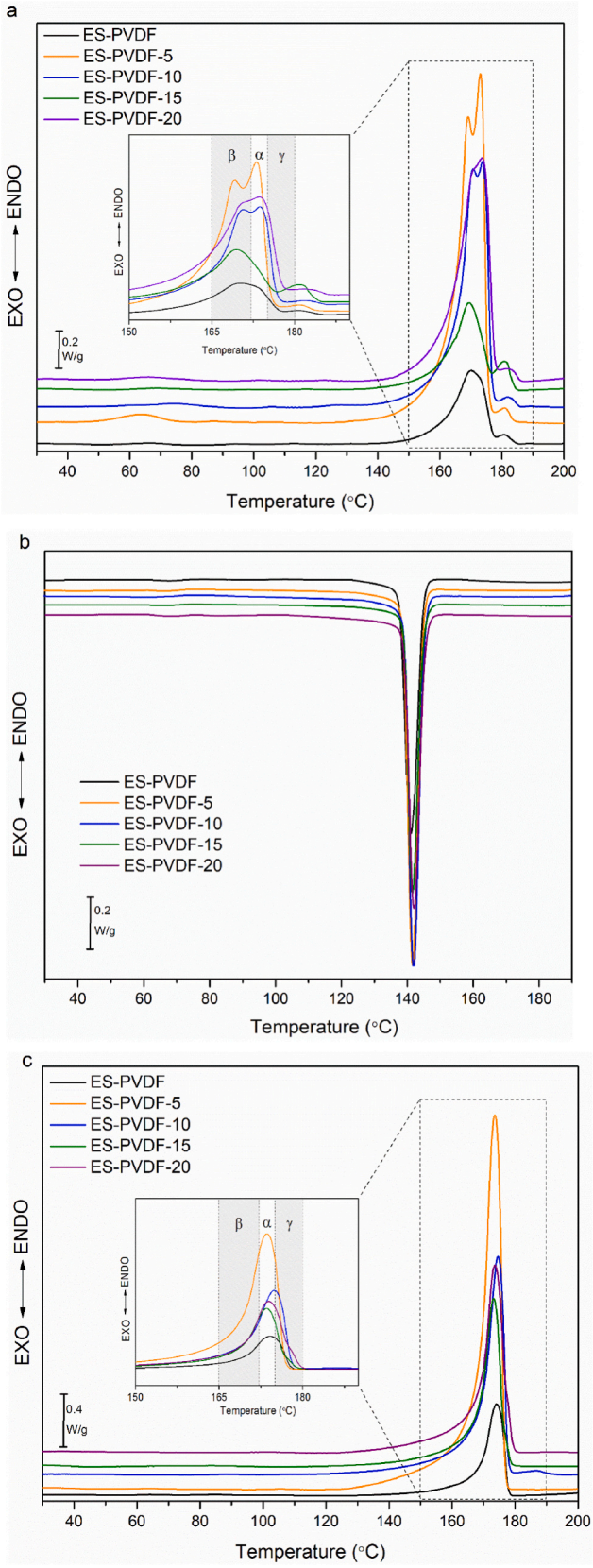

Fig. 7. DSC thermograms of electrospun PVDF/$BaTiO_3$ nanocomposite fibers. DSC first heating scans (a, inset: region 150–200 °C), DSC cooling scans (b) and DSC second heating scans (c, inset: region 150–200 °C).

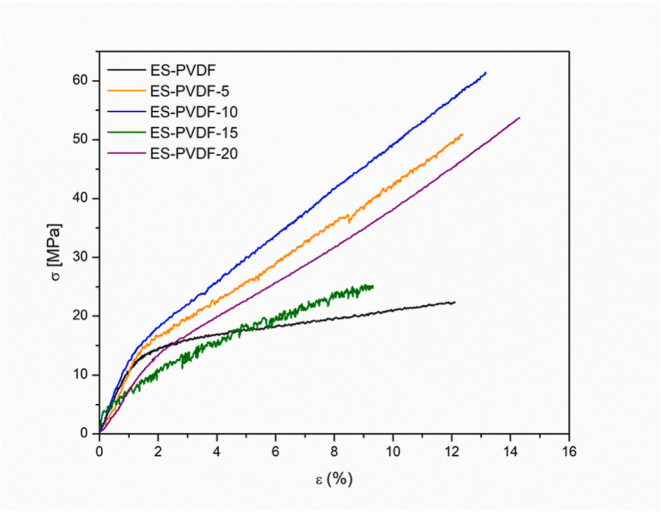

Fig. 8. Stress-strain curves of electrospun PVDF/$BaTiO_3$ nanocomposite fibers.

Table 4
Tensile properties and d_{33} coefficients of PVDF/$BaTiO_3$ nanocomposite fibers.

Sample	Young's modulus [MPa]	σ_{max} [a] [MPa]	$\varepsilon_{\sigma\ max}$ [%]	d_{33} [pC/N]
ES-PVDF	12.00 ± 1.36	24.40 ± 7.69	12.10 ± 10.40	−12.0
ES-PVDF-5	10.30 ± 2.36	54.77 ± 7.49	17.43 ± 4.36	−17.0
ES-PVDF-10	11.35 ± 6.41	53.90 ± 9.66	18.17 ± 12.65	−11.0
ES-PVDF-15	11.57 ± 2.72	36.87 ± 6.27	10.57 ± 3.87	−5.0
ES-PVDF-20	11.77 ± 2.00	55.47 ± 9.93	12.71 ± 0.39	−18.5

[a] Calculated by applying Equation 6.

calculated from the FTIR analysis is almost identical for all composites, but their degrees of crystallinity significantly differ from each other thus affecting the obtained d_{33} values.

Additionally this discrepancy can be attributed to the different degree of crystallinity in the samples calculated by XRD and DSC analysis. Accordingly, the actual β phase content responsible for the piezoelectric performance should be considered as a result of the $F(\beta)$ and X_c values. This value has been referred to as the "content of effective piezo-phase" (C_{ep}) [14,37]. Indeed, if the d_{33} values are combined with C_{ep} values for the composites, a linear fit can be obtained (Fig. 9). Based on these results, it can be concluded that the addition of ceramic nanoparticles did not directly affect the piezoelectric performance of the nanofibers, but rather caused changes in the degree of crystallinity that ultimately led to an increased or decreased d_{33} piezoelectric coefficient.

4. Conclusions

PVDF/$BaTiO_3$ nanocomposites with different content of nano-sized $BaTiO_3$ filler (5, 10, 15, and 20 wt%) were prepared by electrospinning process. In summary, the effects of $BaTiO_3$ nanoparticles content and their distribution on the crystallinity, β phase content, mechanical and piezoelectric properties were investigated in detail. The results showed very high content of electoactive phase F_{EA} (up to 99.4%) in all electrospun samples, giving primary role of the electrospinning process in the development of β phase. Moreover, PVDF/$BaTiO_3$ nanocomposite mats showed improved crystallinity and mechanical properties based on the nucleation ability of the filler. Highest tensile strength (127% higher than ES-PVDF mat) and maximum d_{33} coefficient of 18 pC N^{-1} were determined for nanocomposites containing 20 wt% of $BaTiO_3$.

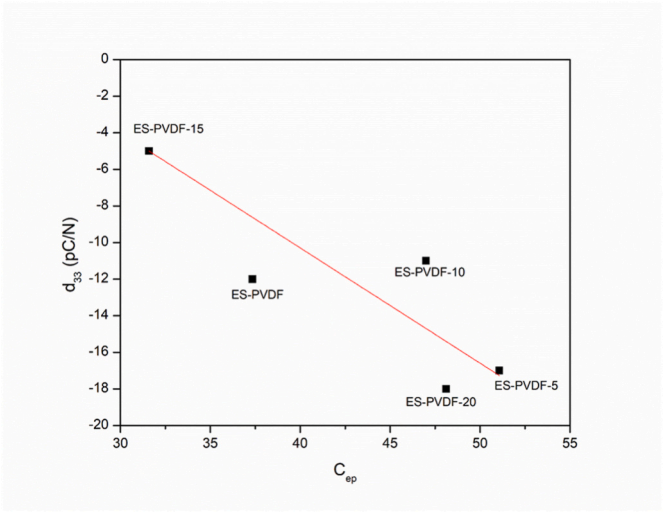

Fig. 9. Dependence of d_{33} piezoelectric coefficient and content of effective piezo-phase (C_{ep}).

Author statement

- The article has not been published previously
- The article is not under consideration for publication elsewhere
- We have no conflicts of interest to disclose
- If accepted, the article will not be published elsewhere in the same form, in any language, without the written consent of the publisher.

Declaration of competing interest

The authors have no competing interest to declare.

Data availability

Data will be made available on request.

Acknowledgements

This work was supported by the NATO grant project (NATO SPS G5772).

References

[1] H. Liu, J. Zhong, C. Lee, S.W. Lee, L. Lin, A comprehensive review on piezoelectric energy harvesting technology: materials, mechanisms, and applications, Appl. Phys. Rev. 5 (2018), https://doi.org/10.1063/1.5074184.
[2] J.S. Park, Electrospinning and its applications, Adv. Nat. Sci. Nanosci. Nanotechnol. 1 (2010) 1–43, https://doi.org/10.1088/2043-6262/1/4/043002.
[3] P. Martins, A.C. Lopes, S. Lanceros-Mendez, Electroactive phases of poly (vinylidene fluoride): determination, processing and applications, Prog. Polym. Sci. 39 (2014) 683–706, https://doi.org/10.1016/j.progpolymsci.2013.07.006.
[4] L. Ruan, X. Yao, Y. Chang, L. Zhou, G. Qin, X. Zhang, Properties and applications of the β phase poly(vinylidene fluoride), Polymers 10 (2018) 1–27, https://doi.org/10.3390/polym10030228.
[5] V. Sencadas, R. Gregorio, S. Lanceros-Méndez, α to β phase transformation and microestructural changes of PVDF films induced by uniaxial stretch, J. Macromol. Sci., Part B: Phys. 48 (2009) 514–525, https://doi.org/10.1080/00222340902837527.
[6] Z. He, F. Rault, M. Lewandowski, E. Mohsenzadeh, F. Salaün, Electrospun PVDF nanofibers for piezoelectric applications: a review of the influence of electrospinning parameters on the β phase and crystallinity enhancement, Polymers 13 (2021) 1–23, https://doi.org/10.3390/polym13020174.
[7] I.S. Chronakis, Novel nanocomposites and nanoceramics based on polymer nanofibers using electrospinning process - a review, J. Mater. Process. Technol. 167 (2005) 283–293, https://doi.org/10.1016/j.jmatprotec.2005.06.053.
[8] T. Lei, L. Yu, G. Zheng, L. Wang, D. Wu, D. Sun, Electrospinning-induced preferred dipole orientation in PVDF fibers, J. Mater. Sci. 50 (2015) 4342–4347, https://doi.org/10.1007/s10853-015-8986-0.
[9] Y. Ahn, J.Y. Lim, S.M. Hong, J. Lee, J. Ha, H.J. Choi, Y. Seo, Enhanced piezoelectric properties of electrospun poly(vinylidene fluoride)/multiwalled carbon nanotube composites due to high β-phase formation in poly(vinylidene fluoride), J. Phys. Chem. C 117 (2013) 11791–11799, https://doi.org/10.1021/jp4011026.
[10] M. Sekkarapatti Ramasamy, A. Rahaman, B. Kim, Effect of phenyl-isocyanate functionalized graphene oxide on the crystalline phases, mechanical and piezoelectric properties of electrospun PVDF nanofibers, Ceram. Int. 47 (2021) 11010–11021, https://doi.org/10.1016/j.ceramint.2020.12.223.
[11] S.A. Haddadi, S.A. Ahmad Ramazani, S. Talebi, S. Fattahpour, M. Hasany, Investigation of the effect of nanosilica on rheological, thermal, mechanical, structural, and piezoelectric properties of poly(vinylidene fluoride) nanofibers fabricated using an electrospinning technique, Ind. Eng. Chem. Res. 56 (2017) 12596–12607, https://doi.org/10.1021/acs.iecr.7b02622.
[12] M. Acosta, N. Novak, V. Rojas, S. Patel, R. Vaish, J. Koruza, G.A. Rossetti, J. Rödel, $BaTiO_3$-based piezoelectrics: fundamentals, current status, and perspectives, Appl. Phys. Rev. 4 (2017), https://doi.org/10.1063/1.4990046.
[13] S. Kalani, R. Kohandani, R. Bagherzadeh, Flexible electrospun PVDF-$BaTiO_3$ hybrid structure pressure sensor with enhanced efficiency, RSC Adv. 10 (2020) 35090–35098, https://doi.org/10.1039/d0ra05675h.
[14] J. Jiang, S. Tu, R. Fu, J. Li, F. Hu, B. Yan, Y. Gu, S. Chen, Flexible piezoelectric pressure tactile sensor based on electrospun $BaTiO_3$/Poly(vinylidene fluoride) nanocomposite membrane, ACS Appl. Mater. Interfaces 12 (2020) 33989–33998, https://doi.org/10.1021/acsami.0c08560.
[15] W. Guo, C. Tan, K. Shi, J. Li, X.X. Wang, B. Sun, X. Huang, Y.Z. Long, P. Jiang, Wireless piezoelectric devices based on electrospun PVDF/$BaTiO_3$ NW nanocomposite fibers for human motion monitoring, Nanoscale 10 (2018) 17751–17760, https://doi.org/10.1039/c8nr05292a.
[16] K. Shi, B. Sun, X. Huang, P. Jiang, Synergistic effect of graphene nanosheet and $BaTiO_3$ nanoparticles on performance enhancement of electrospun PVDF nanofiber mat for flexible piezoelectric nanogenerators, Nano Energy 52 (2018) 153–162, https://doi.org/10.1016/j.nanoen.2018.07.053.
[17] R.S. Sabry, A.D. Hussein, PVDF: ZnO/$BaTiO_3$ as high out-put piezoelectric nanogenerator, Polym. Test. 79 (2019), https://doi.org/10.1016/j.polymertesting.2019.106001.
[18] G. Selleri, M.E. Gino, L. Gasperini, M. Zanoni, C. Gualandi, M.L. Focarete, D. Fabiani, Study on the polarization process for piezoelectric nanofibrous layers, Annu. Rep. - Conf. Electr. Insul. Dielectr. Phenomena, CEIDP (2021) 61–64, https://doi.org/10.1109/CEIDP50766.2021.9705470, 2021-December.
[19] S.H. Oh, I.K. Park, J.M. Kim, J.H. Lee, In vitro and in vivo characteristics of PCL scaffolds with pore size gradient fabricated by a centrifugation method, Biomater. 28 (2007) 1664–1671, https://doi.org/10.1016/j.biomaterials.2006.11.024.
[20] G. Teyssedre, A. Bernes, C. Lacabanne, Influence of the crystalline phase on the molecular mobility of PVDF, J. Polym. Sci., Part B: Polym. Phys. 31 (1993) 2027–2034, https://doi.org/10.1002/polb.1993.090311316.
[21] S.H. Lee, Y.C. Choi, M.S. Kim, K.M. Ryu, Y.G. Jeong, Fabrication and characterization of piezoelectric composite nanofibers based on poly(vinylidene fluoride-co-hexafluoropropylene) and barium titanate nanoparticle, Fibers Polym. 21 (2020) 473–479, https://doi.org/10.1007/s12221-020-9803-1.
[22] Y.J. Kim, C.H. Ahn, M.O. Choi, Effect of thermal treatment on the characteristics of electrospun PVDF-silica composite nanofibrous membrane, Eur. Polym. J. 46 (2010) 1957–1965, https://doi.org/10.1016/j.eurpolymj.2010.08.009.
[23] X. Cai, T. Lei, D. Sun, L. Lin, A critical analysis of the α, β and γ phases in poly (vinylidene fluoride) using FTIR, RSC Adv. 7 (2017) 15382–15389, https://doi.org/10.1039/c7ra01267e.
[24] R. Gregorio, M. Cestari, Effect of crystallization temperature on the crystalline phase content and morphology of poly(vinylidene fluoride), J. Polym. Sci., Part B: Polym. Phys. 32 (1994) 859–870, https://doi.org/10.1002/polb.1994.090320509.
[25] S.F. Mendes, C.M. Costa, C. Caparros, V. Sencadas, S. Lanceros-Méndez, Effect of filler size and concentration on the structure and properties of poly(vinylidene fluoride)/$BaTiO_3$ nanocomposites, J. Mater. Sci. 47 (2012) 1378–1388, https://doi.org/10.1007/s10853-011-5916-7.
[26] Y.L. Liu, Y. Li, J.T. Xu, Z.Q. Fan, Cooperative effect of electrospinning and nanoclay on formation of polar crystalline phases in poly(vinylidene fluoride), ACS Appl. Mater. Interfaces 2 (2010) 1759–1768, https://doi.org/10.1021/am1002525.
[27] R. Hasegawa, Y. Takahashi, Y. Chatani, H. Tadokoro, Crystal structures of three crystalline forms of poly(vinylidene fluoride), Polym. J. 3 (1972) 600–610, https://doi.org/10.1295/polymj.3.600.
[28] I. Pasuk, F. Neațu, Ștefan Neațu, M. Florea, C.M. Istrate, I. Pintilie, L. Pintilie, Structural details of batio3 nano-powders deduced from the anisotropic xrd peak broadening, Nanomaterials 11 (2021), https://doi.org/10.3390/nano11051121.
[29] H.J. Ye, W.Z. Shao, L. Zhen, Crystallization kinetics and phase transformation of poly(vinylidene fluoride) films incorporated with functionalized $BaTiO_3$ nanoparticles, J. Appl. Polym. Sci. 129 (2013) 2940–2949, https://doi.org/10.1002/app.38949.
[30] L. Yu, P. Cebe, Crystal polymorphism in electrospun composite nanofibers of poly (vinylidene fluoride) with nanoclay, Polymer 50 (2009) 2133–2141, https://doi.org/10.1016/j.polymer.2009.03.003.
[31] N. Soin, D. Boyer, K. Prashanthi, S. Sharma, A.A. Narasimulu, J. Luo, T.H. Shah, E. Siores, T. Thundat, Exclusive self-aligned β-phase PVDF films with abnormal piezoelectric coefficient prepared via phase inversion, Chem. Commun. 51 (2015) 8257–8260, https://doi.org/10.1039/c5cc01688f.
[32] Y. Nabata, Molecular motion in form ii poly(Vinylidene fluoride), Jpn. J. Appl. Phys. 29 (1990) 2782–2788, https://doi.org/10.1143/JJAP.29.2782.
[33] K.P. Pramoda, A. Mohamed, I.Y. Phang, T. Liu, Crystal transformation and thermomechanical properties of poly(vinylidene fluoride)/clay nanocomposites, Polym. Int. 54 (2005) 226–232, https://doi.org/10.1002/pi.1692.
[34] M. Khalifa, A. Mahendran, S. Anandhan, Probing the synergism of halloysite nanotubes and electrospinning on crystallinity, polymorphism and piezoelectric

performance of poly(vinylidene fluoride), RSC Adv. 6 (2016) 114052–114060, https://doi.org/10.1039/C6RA20599B.
[35] E. Maccaferri, L. Mazzocchetti, T. Benelli, A. Zucchelli, L. Giorgini, Morphology, thermal, mechanical properties and ageing of nylon 6,6/graphene nanofibers as Nano^2 materials, Compos. B Eng. 166 (2019) 120–129, https://doi.org/10.1016/j.compositesb.2018.11.096.
[36] J. Gomes, J.S. Nunes, V. Sencadas, S. Lanceros-Mendez, Influence of the β-phase content and degree of crystallinity on the piezo-and ferroelectric properties of poly (vinylidene fluoride), Smart Mater. Struct. 19 (2010), https://doi.org/10.1088/0964-1726/19/6/065010.
[37] J. Li, S. Chen, W. Liu, R. Fu, S. Tu, Y. Zhao, L. Dong, B. Yan, Y. Gu, High performance piezoelectric nanogenerators based on electrospun ZnO nanorods/poly(vinylidene fluoride) composite membranes, J. Phys. Chem. C 123 (2019) 11378–11387, https://doi.org/10.1021/acs.jpcc.8b12410.